A SIMULATION STUDY OF THE ELECTRON CLOUD IN THE EXPERIMENTAL REGIONS OF LHC

A. Rossi, G. Rumolo and F. Zimmermann, CERN, Geneva, Switzerland

Abstract

The LHC experimental regions (ATLAS, ALICE, CMS and LHCb) are characterised by having a variable geometry, non-uniform magnetic field, and the presence of two beams that may collide at the Interaction Point (IP). A detailed study of electron multipacting in the experimental chambers is needed to establish the pressure increase due to electron stimulated desorption, especially critical in the experimental regions. Furthermore, knowledge of the predicted electron cloud density all along the experimental regions will allow for an estimation of its possible effects on the beam stability.

1 INTRODUCTION

Photoemission and/or ionisation of the residual gas inside the beam pipe causes production of electrons (as well as of positive ions), which then move under the action of the beam field forces and their own space charge. These primary electrons can initiate a multipacting process, which eventually leads to the build up of a quasi-stationary electron cloud. Positive ions, on the other hand, are not expected to cause major inconveniences, since they have short survival times, low impact energies and a very low equilibrium density compared with that of the electrons [1]. It is supposed that the beam current is lower than the critical current, at which ion-induced pressure instability occurs [2].

In the interaction regions of the LHC (namely at ATLAS, ALICE, and CMS detectors), the maximum acceptable residual gas density is limited by the background noise induced to the detectors by nuclear gas scattering [3, 4, 5]. Electrons accelerated by the beam space charge and impinging on the walls with energies larger than about 10 eV [6] can desorb molecules and contribute to the residual gas density. Moreover, the electron cloud may affect the beam stability and luminosity in collision.

The aim of this study is to evaluate electron cloud build up in the LHC experimental areas and its effects on the residual gas pressure.

The features of the electron cloud build-up are presented and discussed in Sec. 2: electron density saturation value, electron flux to the walls, and energy spectrum of the electrons that hit the wall. Based on these results, for the relevant cases the pressure rise induced by electron desorption is calculated in Sec. 3. In Sec. 4, preliminary results of the code benchmarking are presented, with conclusions in Sec. 5.

2 ELECTRON CLOUD BUILD-UP

2.1 LHC experimental regions layout

An example of layout of experimental beam vacuum chambers is given in Fig. 1. The experimental chambers differ from the standard arc chambers mainly because of their variable geometry, the non-uniform magnetic fields, and the two beams travelling in opposite directions. Practically all the experimental chambers are at room temperature and they are coated with low activation sputtered TiZrV Non-Evaporable Getters (NEG's) [7]. The TiZrV NEG has been chosen, among other reasons, because it can limit electron multipacting due to its low Secondary Emission Yield (SEY). It was found that, after only 200°C activation, the maximum SEY, δ_{max}, becomes about 1.1 for incident electron energies between 300 and 400 eV [8]. The SEY remains below 1.2 even after saturation of the NEG surface with CO or water vapour [9]. However, after a few air venting/activation cycles, the maximum SEY can increase up to $\delta_{max} \sim 1.4$ [10].

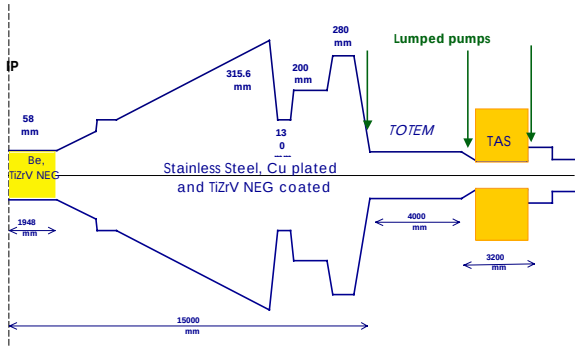

Figure 1: CMS-TOTEM beam pipe layout

2.2 Electron cloud simulation parameters

As the experiments are supposed to run independently of one another, we cannot rely on the experimental solenoid field (in the central sections of ATLAS and CMS) to prevent multipacting. Therefore, the simulations have been carried out assuming field free regions, which is the worst case.

The study of multipacting in the experimental regions has been conducted using ECLOUD [11] and considering the following set of parameters and/or assumptions:

1. The maximum SEY is 1.1 or 1.4.
2. We have assumed the elastic reflection to occur as on the copper samples recently measured [12]. Elastic reflection is anyway strongly dependent on the surface roughness more than on the material on which the electrons impinge.
3. The photon flux to the wall for the LHC geometry has been evaluated using the code developed by F. Zimmermann [13]. We expect the photon flux in the straight experimental areas to be sensibly smaller than the one in the arcs.
4. Bunch transverse sizes have been taken at injection and at top energy, both at the interaction points and up to 20m downstream. The study shows, that there is no strong dependence of the electron multipacting on this parameter. This was predictable since for the cases considered, the beam was much smaller than the pipe cross section.
5. The two cases of two beams reaching a selected location simultaneously (25ns bunch spacing and double bunch intensity) and two beams at half distance (12.5ns bunch spacing and single bunch nominal intensity) have been simulated.
6. Geometry variable in steps from the smallest to the largest diameter for each experimental region.
7. The effects of RF traps in enlarged sections of the chambers have not been taken into account.

Table 1. LHC parameters assumed in the electron cloud simulations

	symbol	value
bunch proton population	N_b	1.05×10^{11}
bunch spacing		7.48 m
r.m.s. bunch length		7.5 cm
proton energy		7 TeV
primary ph-e rate per photon		2.98×10^{-7}
Reflectivity		10%
max secondary emission yield	SEY	1.1 and 1.4
energy of max SEY		300 eV
energy distr. for sec. Electrons		Gaussian
r.m.s. horizontal beam size		15.86 - 444 μm
r.m.s. vertical beam size		"
radial half aperture		22 to 200 mm

2.3. Simulation results: electron density and flux to the wall

The electron line density (e^-/m) and flux to the wall (e^-/s/m) are displayed in Fig. 2, 3 and 4 for different chamber radii, and for SEY = 1.4. It can be observed that, despite the low value of SEY, there is an electron cloud build up. Both the rise time and saturation values depend on the chamber radius. No obvious correlation was found.

In Fig. 5, the saturation values of the electron flux to the wall per unit wall area (e^-/s/cm^2), with SEY = 1.1 and SEY = 1.4 are compared. The saturation levels appear to be more sensitive to a variation of SEY for radii > 70 mm. For the calculations of the residual gas density it was assumed that the electron flux to the wall is a step function, given the shape of the curves and that the two cases considered (simultaneous arrival and half bunch spacing) should correspond to the extreme cases. The values used are shown in Fig. 5, with blue dotted lines.

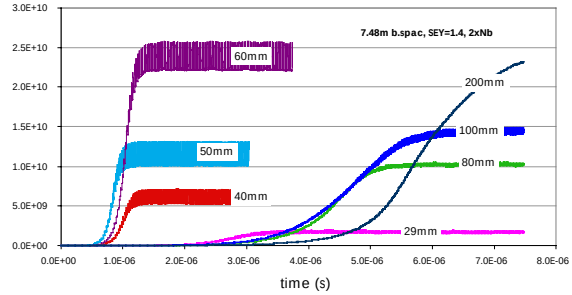

Figure 2: Time evolution of the electron line density (e^-/ m) for different chamber radii, for two beams arriving simultaneously (nominal bunch spacing and double bunch current).

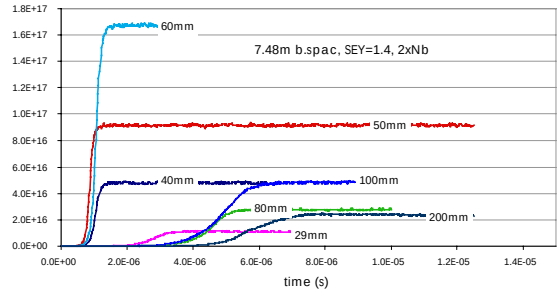

Figure 3: Time evolution of the electron flux to the wall (e^-/s/m) for different chamber radii, for two beams arriving simultaneously (nominal bunch spacing and double bunch current).

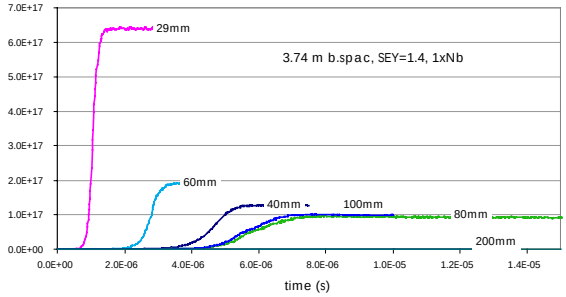

Figure 4: Time evolution of the electron flux to the wall (e^-/s/m) for different chamber radii, for two beams at half nominal bunch spacing and bunch current.

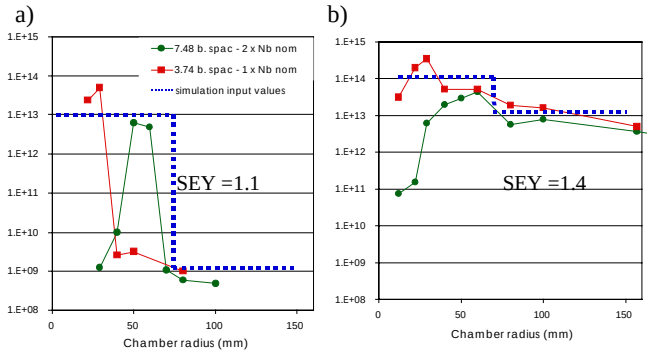

Figure 5: Saturation value of the electron flux to the wall ($e^-/s/cm^2$) as a fuction of the chamber radius, and the values used for the calculations of the gas density in the experimental regions. a) SEY = 1.1; b) SEY = 1.4.

2.4. Simulation results: electron impact energy distribution at the wall

The electron impact energy distribution at the wall is displayed in Fig. 6 for the two cases of beams arriving simultaneously and with half nominal bunch spacing. The maximum impact energy varies between 2.5 keV for the latter case and 4.5 keV for simultaneous beams (which corresponds to twice the bunch current). Both figures display an energy range from 0 to 160 eV to show that a non negligible fraction of the electrons impinge on the walls with an energy larger than 10 eV, that is larger than the threshold energy for stimulated gas desorption [6].

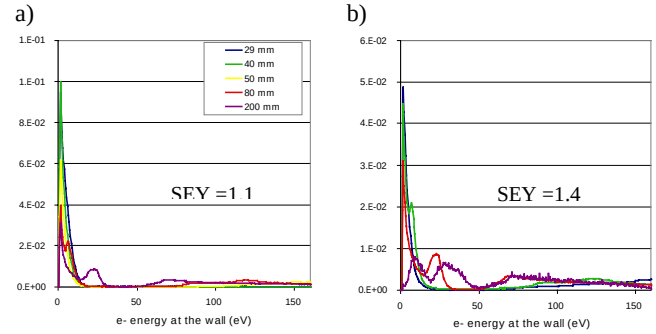

Figure 6: Electron energy distribution at the wall (eV). a) beams arriving simultaneously, with double current. b) beam at half of the nominal bunch spacing and nominal current.

3 MOLECULAR DENSITY ESTIMATION IN THE EXPERIMENTAL REGIONS

3.1. Molecular density estimation parameters

As mentioned in the previous section, a large fraction of the electrons impinging on the wall will cause gas desorption. The Electron Stimulated Desorption yield (ESD) depends on the impact energy [6]. The values for ESD used for the estimates of the residual gas density are listed in Table 2 for TiZrV coating [14]. Since the ESD varies by a factor of ~ 2 between 100 and 300 eV, and given the spread of measured data in the literature, a constant value for all energies was assumed.

Table 2 also contains other parameters relevant for the molecular density estimations, such as the Photon Stimulated gas Desorption (PSD) from TiZrV NEG coating and its sticking coefficients. It should be noted that the desorption yields from NEG coating are reached with other materials after a long conditioning (about 1 year LHC beam time).

Table 2. LHC parameters assumed in the residual gas density estimations for the TiZrV NEG coating

Desorption Yield	H_2	CH_4	CO	CO_2
PSD[i]	2.5×10^{-7}	2.5×10^{-9}	1.25×10^{-8}	1.25×10^{-8}
ESD[ii] [14]	2.0×10^{-4}	5.0×10^{-6}	1.0×10^{-4}	1.0×10^{-4}
Sticking Coefficient				
Freshly activated NEG[iii] [7]	5.0×10^{-3}	0	1.0×10^{-1}	1.0×10^{-1}
Cycled NEG[iv] [7]	5.0×10^{-4}	0	1.0×10^{-2}	1.0×10^{-2}

[i] Corrected for grazing incidence (factor of 5 larger at grazing incidence [15] than perpendicular incidence [16]) and considering the expected 12eV critical energy at the LHC interaction regions [17].

[ii] ~500eV incident energy.

[iii] Corresponding to SEY = 1.1.

[iv] Cycled = exposed to air at atmospheric pressure and reactivated several (~ 10) times. SEY = 1.4.

3.2 Results

The density profiles for the ATLAS and CMS (with TOTEM) experimental beam pipe are presented in Fig. 7 and 8. The 'static' density (Fig. 7.1 a) and 8.1, a)) is estimated for a freshly activated NEG coating and is compared to the expected values during proton beam operations (SEY = 1.1, Fig. 7.1 b) and 8.1, b)). It should be noted that the major contribution to the gas density is given by electron induced desorption, since photon induced desorption is at least 2 orders of magnitude smaller. In both cases, the main gas species is methane. The ATLAS beam pipe has a smaller cross section, which accounts for the higher density of CH_4, whose pumping is conductance limited.

After the NEG coating has been exposed to air at atmospheric pressure (due for example to maintenance works) and reactivated for about 10 times, the δ_{max} increases to ~ 1.4 with a consequent increase of the electron cloud activity, as detailed in section 2. At the same time, the sticking coefficients, and therefore the distributed pumping, is reduced to about one tenth of the initial value. Both phenomena lead to a further increase in the molecular density as shown in Fig. 7.2 and 8.2. The hydrogen density is now comparable to that of methane,

since the distributed pumping speed for hydrogen is low, while the pumping of methane is not affected by the NEG deterioration.

Note that, beyond 22 m from the IP, the surface is supposed to be at cryogenic temperature. Here, the distributed pumping is effective for methane, but lower than the NEG pumping for the other gas species.

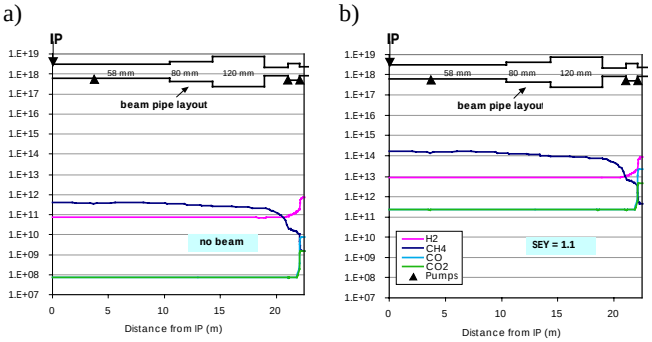

Figure 7.1 : ATLAS experiment. Molecular density distribution (molecules/m^3) as a function of the distance from the experiment interaction point (IP) for a freshly activated TiZrV NEG coating. a) : no running beam (static). b) : density rise due to electron desorption (main contribution) with SEY = 1.1.

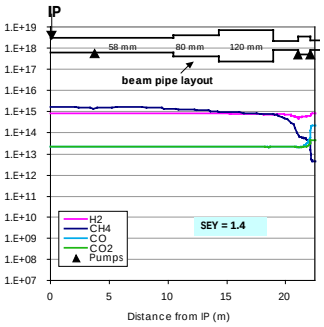

Figure 7.2 : ATLAS experiment. Molecular density distribution (molecules/m^3) as a function of the distance from IP. The pressure increase due to electron desorrption (main contribution) with SEY = 1.4 and 1/10 of NEG pumping.

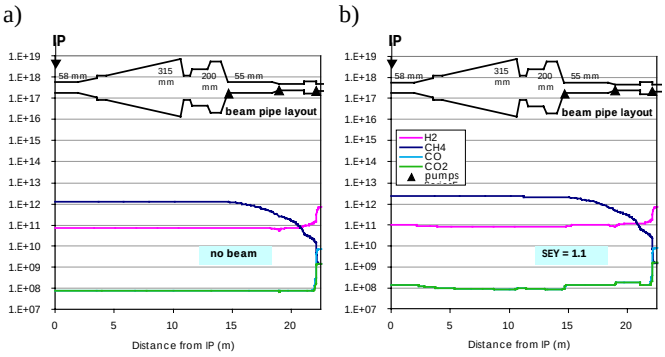

Figure 8.1 : CMS experiment. . Molecular density distribution (molecules/m^3) as a function of the distance from the IP for a freshly activated TiZrV NEG coating. a) : no running beam (static). b) : density rise due to electron desorption (main contribution) with a SEY = 1.1.

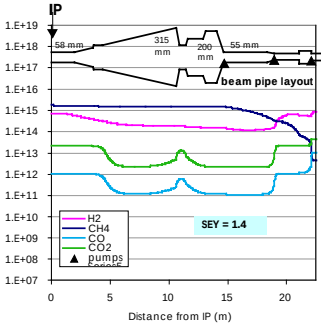

Figure 8.2 : CMS experiment. Molecular density distribution (molecules/m^3) as a function of the distance from the experiment interaction points (IP). The density increase due to electron desorrption (main contribution) is shown for a SEY = 1.4 and 1/10 of the initial NEG pumping.

The profile of the CO and CO_2 gas density in the CMS geometry results from a larger electron flux to the wall in the smaller cross sections (as detailed in Sect. 2.3) and a reduced NEG pumping (which is proportional to the pipe surface area).

4. BENCHMARKING

If the quantitative results of the electron cloud simulations are correct, the main contribution to the residual gas density comes from electron induced gas desorption, as it was explained in the previous section. Since these values are used to assess the validity of the experimental beam chambers design, benchmarking of the simulation results against experimental data is urgently needed. For example, for the CMS experiment, the background noise corresponding to the density levels estimated for SEY = 1.4 is very close to the maximum value the detector can tolerate [18].

In this section, preliminary results of the electron cloud code benchmarking are presented. The time evolution curves of the electron build-up signal [19] (negative voltage) during experiments in the CERN SPS with LHC type proton beam (25 ns bunch spacing) are compared with the simulation results. The data cannot be converted into number of electrons collected by the pick-up per second, because the instrument was not calibrated prior to the run. In Fig. 9.a) the electron build-up was measured with a train of 72 bunches, 8.3×10^{10} protons/bunch. The pressure measured was about 2×10^{-7} Torr.

The input data for the simulations that best reproduce the experimental data are listed in Table 3. It was assumed that the primary electrons are created by ionisation of the residual gas by the proton beam, as it should be in the SPS. The beam structure and the values assumed for the gas pressure were the same as recorded during the experiments.

Table 3. LHC parameters assumed in the electron cloud simulations for the benchmarking

	value
bunch proton population	8.3×10^{10}
bunch spacing	7.48 m
r.m.s. bunch length	30 cm
proton energy	26 GeV
residual gas pressure	2×10^{-7} and 4×10^{-8} Torr
gas ionisation cross section	2 MBarn
max secondary emission yield	1.6
energy of max SEY	300 eV
energy distr. for sec. electrons	Gaussian
r.m.s. horizontal beam size	444 μm
r.m.s. vertical beam size	"
radial half horizontal aperture	76 mm
radial half vertical aperture	17.5 mm

The time evolution of the experimental data are well reproduced by the simulations. In Fig. 9.a) the flux of electrons incident on the pick up is plotted as a function of time. In Fig. 9.b), the electron line density resulting from the simulations is displayed.

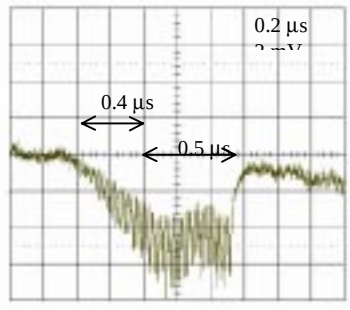

a)

Courtesy of M. Jimenez [19]

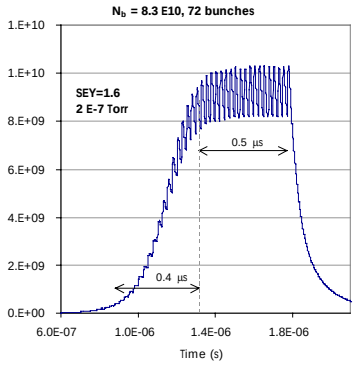

b)

Figure 9: Time evolution with a train of 72 bunches. The the experimental data (electron flux to the wall, a) are compared to simulation results (electron line density, b).

5 CONCLUSIONS AND FUTURE WORK

The variation of the electron cloud activity with radius (as for the LHC experimental beam pipe geometry) and SEY characteristic of TiZrV NEG coating have been simulated using ECLOUD. The results of the simulations have been used as input to estimate the residual gas density in the interaction regions during proton beam running. It was found that, despite the low SEY of the TiZrV NEG coating after activation, the levels of electron flux to the wall at saturation can induce a gas desorption which will dominate the residual gas density.

Benchmarking of the simulation results are promising. Further effort should be put into this to validate quantitatively the code results so as to use it as a design tool.

The effects of the electron cloud on the beam dynamics are to be analysed.

6 REFERENCES

[1] G. Rumolo and F. Zimmermann, CERN-SL-2001-014-AP.

[2] A. Mathewson, Maui, Hawai, November 3-9, 1994.

[3] ALICE Technical Proposal, CERN/LHCC/95-71.

[4] ATLAS TDR 13, CERN/LHCC/99-01.

[5] CMS Technical Proposal, CERN/LHCC/94-38.

[6] G. Vorlaufer, N. Hilleret, F. Billard, CERN Vac. Tech. Note 00-32.

[7] C. Benvenuti et al., Vacuum 60 (2001) 57-65.

[8] C. Scheuerlein et al., CERN EST/2000-07 (SM).

[9] B. Henrist et al., CERN Vac. Tech. Note 98-08.

[10] B. Henrist and C. Scheuerlein, CERN Vac. Tech. Note 98-20.

[11] G. Rumolo and F. Zimmermann, same proceedings.

[12] V. Baglin, I. Collins, B. Henrist, N. Hilleret, G. Vorlaufer, CERN, LHC-Project-Report-472.

[13] F. Zimmermann, CERN, LHC Project Report 237 (2000).

[14] C. Benvenuti, P. Chiggiato, F. Cicoira, V. Rouzinov, Vacuum 50 N. 1-2 (1998) 57-63.

[15] O. Gröbner, A.G. Mathewson, H. Störi, P. Strubin, R. Souchet, Vacuum 33, N. 7 (1983) 397-406

[16] V. Baglin, C. Benvenuti, P. Costa Pinto, P. Chiggiato, N. Hilleret, A. Rossi, presented at IVC 15, San Francisco, Nov 2001.

[17] J. Gómez-Goñi et al., J. Vac. Sci. Technol. A 12(4) Jul/Aug 1994.

[18] M. Huhtinen, CMS-TOTEM beam pipe EDR, CERN, April 2002.

[19] M. Jimenez et al., proceedings of 11th Chamonix workshop, 2001.